Mathematical Models and Methods in Applied Sciences
Vol. 5, No. 8 (1995) 1113–1128

A FOUR-NODE QUADRILATERAL MIXED-INTERPOLATED ELEMENT FOR SOLIDS AND FLUIDS

DANIEL PANTUSO* and KLAUS-JÜRGEN BATHE†
Massachusetts Institute of Technology, Cambridge, MA 02139, USA

Communicated by F. Brezzi
Received 1 December 1994

A four-node quadrilateral element is presented which shows promise for general compressible and incompressible two-dimensional analysis of solids and fluids. The element is based on a mixed interpolation of displacements (velocities), pressure and strains (velocity strains). We show that the element satisfies a numerical inf-sup test, and give results of some analysis problems that demonstrate the capabilities of the element.

1. Introduction

Much research effort has been spent to obtain an effective four-node quadrilateral finite element for the analysis of two-dimensional structural problems and fluid flows.

Considering structural analysis, the element should have high predictive capabilities in bending action, and should not lose its predictive capabilities when almost incompressible conditions are encountered.[1] Quite efficient four-node structural elements for plane stress analysis have been published[5–8] but these elements are not sufficiently effective in almost incompressible conditions.

Considering fluid flow solutions, the element should be applicable to incompressible fluids flows. If we have an element that is effective in the analysis of incompressible solids, we can employ the same element formulation also for fluids at low Reynolds numbers by simply using in the formulation velocities instead of displacements. We shall therefore develop our element here for structural analysis, but for fluid flow solutions see Secs. 4.2 and 4.3.

The mathematical condition that we would like our element to satisfy is the inf-sup condition for incompressible analysis.[1,2] To investigate whether the element satisfies the inf-sup condition we have implemented a numerical inf-sup test.[3] The proposed element passes this test but of course a rigorous analytical proof would be very desirable.

*Graduate Student

†Professor of Mechanical Engineering

In what follows we present in detail the quadrilateral element for two-dimensional plane stress and plane strain analyses, and also mention briefly the corresponding axisymmetric element and three-dimensional eight-node brick element. In Sec. 3 we discuss the implementation of the inf-sup test and give results obtained when applied to our element. In Sec. 4 we present the results of some standard analysis problems to show the capabilities of the element.

2. Theoretical Foundation and Interpolations

In this section we first present the variational principle that forms the basis of the element formulation and then give the interpolations used.

As mentioned earlier, we consider the structural analysis problem but the development is also directly applicable to fluid flow solutions.

2.1. *Variational formulation*

Let B be a general body in space with prescribed displacements over the boundary S_u, applied tractions over S_f and $S_u \cap S_f = \emptyset$. The material response is assumed to be represented by a polyconvex stored energy function $W(\mathbf{x}, \boldsymbol{\varepsilon})$, where $\mathbf{x}$ indicates material points and $\boldsymbol{\varepsilon}$ denotes the strain tensor. Although, in the following, we will refer to linear isotropic elasticity, the generality of the variational principle renders our results applicable to any solid provided the corresponding expression of the stored energy function is used.

Let us consider the following variational indicator[1]:

$$\Pi^*(\mathbf{u}, p) = \int_V \left[\frac{1}{2}\, \boldsymbol{\varepsilon}' \cdot \mathbf{C}' \cdot \boldsymbol{\varepsilon}' + \frac{1}{2}\frac{p^2}{\kappa} - p\left(\frac{p}{\kappa} + \varepsilon_v\right) \right] dV - \mathcal{R}(\mathbf{u}), \tag{1}$$

where $\mathbf{u}$ denotes the displacement field, $\boldsymbol{\varepsilon}'$ and ε_v are, respectively, the deviatoric and volumetric part of the strain tensor $\boldsymbol{\varepsilon}$, p is the pressure, $\mathbf{C}'$ is the stress-strain matrix for the deviatoric components of stress and strain and κ is the bulk modulus. The term $\mathcal{R}(\mathbf{u})$ accounts for the externally applied body forces $\mathbf{f}^B$ and surface tractions $\mathbf{f}^{S_f}$,

$$\mathcal{R}(\mathbf{u}) = \int_V \mathbf{u} \cdot \mathbf{f}^B dV + \int_{S_f} \mathbf{u}^{S_f} \cdot \mathbf{f}^{S_f} dS_f\,. \tag{2}$$

Inspired by the developments given in Refs. 6 and 7, we write the strain field as,

$$\boldsymbol{\varepsilon} = \partial_\varepsilon \mathbf{u} + \tilde{\boldsymbol{\varepsilon}}\,, \tag{3}$$

where $\partial_\varepsilon \mathbf{u}$ is the strain corresponding to the displacement field $\mathbf{u}$ and $\tilde{\boldsymbol{\varepsilon}}$ represents an enhancement in the strain field. The deviatoric and the volumetric strains are

$$\boldsymbol{\varepsilon}' = \partial_{\varepsilon'} \mathbf{u} + \tilde{\boldsymbol{\varepsilon}}'\,, \tag{4}$$

$$\varepsilon_v = \partial_{\varepsilon_v} u + \tilde{\varepsilon}_v\,. \tag{5}$$

Substituting Eqs. (4) and (5) into Eq. (1), we obtain

$$\tilde{\Pi}(\mathbf{u},\tilde{\varepsilon},p)=\int_V\left[\frac{1}{2}(\partial_{\varepsilon'}\mathbf{u}+\tilde{\varepsilon}')\cdot\mathbf{C}'\cdot(\partial_{\varepsilon'}\mathbf{u}+\tilde{\varepsilon}')-\frac{1}{2}\frac{p^2}{\kappa}-p(\partial_{\varepsilon_v}u+\tilde{\varepsilon}_v)\right]dV-\mathcal{R}(\mathbf{u})\,. \tag{6}$$

Note that we obtain the stress tensor τ as

$$\tau=\boldsymbol{\tau}'-p\,\boldsymbol{\delta}\,, \tag{7}$$

where the deviatoric part is

$$\boldsymbol{\tau}'=\mathbf{C}'(\partial_{\varepsilon'}\mathbf{u}+\tilde{\varepsilon}') \tag{8}$$

and $\boldsymbol{\delta}$ is the unit second-order tensor.

Invoking stationarity of $\tilde{\Pi}$ we obtain the following governing variational equations:

$$\begin{aligned}
&\int_V[\partial_{\varepsilon'}\delta\mathbf{u}\cdot\mathbf{C}'\cdot(\partial_{\varepsilon'}\mathbf{u}+\tilde{\varepsilon}')-(\partial_{\varepsilon_v}\delta u)\;p]\,dV-\delta\mathcal{R}(\mathbf{u})=0\,,\\
&\int_V[\delta\tilde{\varepsilon}'\cdot\mathbf{C}'\cdot(\partial_{\varepsilon'}\mathbf{u}+\tilde{\varepsilon}')-p\,\delta\tilde{\varepsilon}_v]\,dV=0\,,\\
&\int_V\left[-\delta p(\frac{p}{\kappa}+(\partial_{\varepsilon_v}u+\tilde{\varepsilon}_v))\right]\,dV=0\,.
\end{aligned} \tag{9}$$

The first entry of Eqs. (9) gives the well-known equilibrium equation and the last one gives the relation between pressure and volumetric strains. Since we know that the stress field cannot be zero under the action of externally applied loads, the second equation imposes conditions to the enhanced strain field, which means that it cannot be arbitrarily selected. In fact, for the constant stress field case (patch test) the second entry of Eqs. (9) becomes,

$$\tau\cdot\int_V\delta\tilde{\varepsilon}\,dV=0 \tag{10}$$

which means that the integral of the enhanced strain field must vanish. We will choose our finite element interpolations of the enhanced strain field such that condition (10) is satisfied and will refer to this point in more detail in the following section.

2.2. *Element interpolations*

The geometry and the displacement field are described using the standard four-node isoparametric interpolations

$$\mathbf{x}=\sum_{i=1}^{4}h_i(\mathbf{r})\mathbf{x}_i\,, \tag{11}$$

$$\mathbf{u}=\sum_{i=1}^{4}h_i(\mathbf{r})\mathbf{u}_i\,. \tag{12}$$

In these equations, h_i are the usual interpolation functions, $\mathbf{r}$ indicates the isoparametric coordinates, and $\mathbf{x}_i$ and $\mathbf{u}_i$ are the nodal point coordinates and nodal point displacements, respectively. The deviatoric and volumetric strains corresponding to $\mathbf{u}$ are

$$\partial_{\varepsilon'}\mathbf{u} = \mathbf{B}'(\mathbf{r})\,\hat{\mathbf{u}}\,, \tag{13}$$

$$\partial_{\varepsilon_v}\mathbf{u} = \mathbf{B}_v(\mathbf{r})\,\hat{\mathbf{u}}\,, \tag{14}$$

where $\mathbf{B}'(\mathbf{r})$ and $\mathbf{B}_v(\mathbf{r})$ are, respectively, the corresponding strain interpolation matrices and $\hat{\mathbf{u}}$ contains the nodal point displacements.

The interpolations of the pressure field and the enhanced strain field play an important role in the element formulation. As is well known, using the bilinear displacement interpolation and no enhanced strain field (that is, using $\tilde{\varepsilon} = \mathbf{0}$), the "best" element is the displacement/constant pressure element (the 4/1 or Q1-P0 element). Any higher order pressure interpolation will weaken the performance of the element in almost incompressible analysis, and even the constant pressure element is not reliable (unless used in certain macro-element patterns). The 4/1 element does not satisfy the inf-sup condition. See Refs. 1 and 2 for further discussions of this element.

We are using the enhancement in the strain field to increase the predictive capability of the element in bending and enlarge at the same time the "divergence space" of the element. Based on these thoughts, we propose to use the same interpolation for the pressure as for the displacements, that is

$$p = \sum_{i=1}^{4} h_i(\mathbf{r})\,p_i = \mathbf{H}(\mathbf{r})\hat{\mathbf{p}}\,, \tag{15}$$

where the p_i are the nodal point pressure values.

Hence the element will yield a continuous pressure field across the element boundaries.

With the above displacement and pressure interpolations it is now crucial to select an appropriate strain field $\tilde{\varepsilon}$.

Let us define the enhanced strain field interpolation as

$$\tilde{\varepsilon} = \mathbf{G}(\mathbf{r})\boldsymbol{\alpha}\,. \tag{16}$$

The matrix $\mathbf{G}(\mathbf{r})$ (to be defined in detail) contains functions of $\mathbf{r}$ and the vector $\boldsymbol{\alpha}$ contains the internal element parameters.

Using Eqs. (11) to (16) in Eqs. (9) we obtain the following discrete finite element equations,

$$\begin{pmatrix} \mathbf{K}_{uu} & \mathbf{K}_{u\alpha} & \mathbf{K}_{up} \\ \mathbf{K}_{u\alpha}^T & \mathbf{K}_{\alpha\alpha} & \mathbf{K}_{\alpha p} \\ \mathbf{K}_{up}^T & \mathbf{K}_{\alpha p}^T & \mathbf{K}_{pp} \end{pmatrix} \begin{pmatrix} \hat{\mathbf{u}} \\ \boldsymbol{\alpha} \\ \hat{\mathbf{p}} \end{pmatrix} = \begin{pmatrix} \mathbf{R} \\ \mathbf{0} \\ \mathbf{0} \end{pmatrix}, \tag{17}$$

where

$$\mathbf{K}_{uu} = \int_V \mathbf{B}'^T(\mathbf{r})\mathbf{C}'\mathbf{B}'(\mathbf{r})dV\,, \qquad \mathbf{K}_{up} = -\int_V \mathbf{B}_v^T(\mathbf{r})\mathbf{H}(\mathbf{r})dV\,,$$
$$\mathbf{K}_{pp} = -\int_V \frac{1}{\kappa}\,\mathbf{H}^T(\mathbf{r})\mathbf{H}(\mathbf{r})dV\,, \qquad \mathbf{K}_{\alpha p} = -\int_V \mathbf{G}_v^T(\mathbf{r})\mathbf{H}(\mathbf{r})dV\,, \tag{18}$$
$$\mathbf{K}_{\alpha\alpha} = \int_V \mathbf{G}'^T(\mathbf{r})\mathbf{C}'\mathbf{G}'(\mathbf{r})dV\,, \qquad \mathbf{K}_{u\alpha} = \int_V \mathbf{B}'^T(\mathbf{r})\mathbf{C}'\mathbf{G}'(\mathbf{r})dV$$

and $\mathbf{R}$ is the usual load vector.

The final stiffness matrix is obtained by statically condensing out the internal parameters $\boldsymbol{\alpha}$ at the element level.

The matrix $\mathbf{G}(\mathbf{r})$ must satisfy the requirement that the linear system of equations (17) be solvable, that is, after elimination of the physical rigid body modes. We also want the element to pass the patch test.

Of course, satisfying these requirements does not assure that we have a stable finite element discretization. However, this solvability condition is necessary and the passing of the patch test indicates whether the element will be useful. Ideally, as mentioned above, we would be able to analytically show that the element formulation satisfies the inf-sup condition for incompressible analysis.

The system of equations (17) will be solvable if the matrix $\mathbf{K}_{\alpha\alpha}$ is invertible which is guaranteed if the columns of the matrix $\mathbf{G}(\mathbf{r})$ are linearly independent. According to our variational principle, the integral of $\tilde{\varepsilon}$ over the volume of the element must vanish. Hence, assuming a constant thickness we must have

$$\int_{-1}^{+1}\int_{-1}^{+1} \mathbf{G}(\mathbf{r})J(\mathbf{r})d\mathbf{r} = 0\,, \tag{19}$$

where $J(\mathbf{r})$ is the Jacobian determinant for the transformation from the physical coordinates (x, y) to the isoparametric coordinates (r, s).

We will now establish the enhanced strain interpolation defined in Eq. (16). Let us consider first a square element of size 2×2. In this case we use $\mathbf{G}(\mathbf{r})$=$\mathbf{G}^*(\mathbf{r})$,

$$\mathbf{G}^*(\mathbf{r}) = \begin{pmatrix} r & 0 & 0 & 0 & rs & 0 \\ 0 & s & 0 & 0 & 0 & rs \\ 0 & 0 & r & s & 0 & 0 \end{pmatrix}. \tag{20}$$

Note that the first four columns of $\mathbf{G}^*(\mathbf{r})$ define the strain interpolations that actually correspond to the incompatible displacement interpolations used in the element of Wilson.[7] The two columns that we add in $\mathbf{G}^*(\mathbf{r})$ enable the element to pass the numerical inf-sup test given in Sec. 3.

If the element is a general quadrilateral we need to transform the strains in the isoparametric coordinate system to the physical coordinate system and we perform

this tensor transformation in matrix form,

$$\mathbf{G}(\mathbf{r}) = \frac{J_0}{J(\mathbf{r})}\bar{\mathbf{X}}_0\mathbf{G}^*(\mathbf{r}), \tag{21}$$

where

$$\bar{\mathbf{X}}_0^{-1} = \begin{pmatrix} X_{0_{11}}^2 & X_{0_{21}}^2 & X_{0_{11}}X_{0_{21}} \\ X_{0_{12}}^2 & X_{0_{22}}^2 & X_{0_{12}}X_{0_{22}} \\ 2X_{0_{12}}X_{0_{11}} & 2X_{0_{21}}X_{0_{22}} & X_{0_{11}}X_{0_{22}} + X_{0_{12}}X_{0_{21}} \end{pmatrix} \tag{22}$$

and

$$\mathbf{X}_0 = \left.\frac{\partial \mathbf{x}(r)}{\partial \mathbf{r}}\right|_{\mathbf{r}=\mathbf{0}} \quad \text{and } J_0 = J|_{\mathbf{r}=\mathbf{0}}. \tag{23}$$

Hence, we use in Eq. (21) the geometry gradient and determinant evaluated at the center of the element. Since the condition (19) is satisfied for the square element, the same condition is also satisfied for the element of general geometric shape.

We note that, of course, higher order terms can be included in the strain interpolation matrix $\mathbf{G}^*(\mathbf{r})$ provided condition (19) is satisfied. However, we performed some numerical experimentation which showed that no significant improvements are obtained by including higher order terms.

2.3. *The axisymmetric and three-dimensional cases*

For axisymmetric analysis due to the hoop strain and the presence of the factor $x_r(\mathbf{r})$ (the radius expressed as a function of the natural coordinates) in the integrations, some extensions of the above element formulation are needed.

To include an enhancement for the hoop strain we modify the enhanced strain interpolation (20). Consider the 2×2 element and the interpolation matrix

$$\tilde{\mathbf{G}}^*(\mathbf{r}) = \begin{pmatrix} r & 0 & 0 & 0 & rs & 0 \\ 0 & s & 0 & 0 & 0 & rs \\ 0 & 0 & r & s & 0 & 0 \\ 0 & 0 & 0 & 0 & rs & rs \end{pmatrix}. \tag{24}$$

Using $\tilde{\mathbf{G}}^*(\mathbf{r})$, condition (19) is violated due to the additional thickness factor $x_r(\mathbf{r})$ in the integral and a normalization of the interpolation (24) is required.

Let

$$\mathbf{G}^*(\mathbf{r}) = \tilde{\mathbf{G}}^*(\mathbf{r}) + \tilde{\mathbf{G}}_c^*, \tag{25}$$

where $\tilde{\mathbf{G}}_c^*$ is a correction matrix of constant elements which satisfy Eq. (19). Then we obtain

$$\mathbf{G}^*(\mathbf{r}) = \tilde{\mathbf{G}}^*(\mathbf{r}) - \frac{1}{\int_{-1}^{1}\int_{-1}^{1} x_r(\mathbf{r})d\mathbf{r}} \int_{-1}^{1}\int_{-1}^{1} \tilde{\mathbf{G}}^*(\mathbf{r})x_r(\mathbf{r})d\mathbf{r}. \tag{26}$$

The matrix $\mathbf{G}(\mathbf{r})$ for a general quadrilateral element is then obtained by the transformations defined in Eqs. (21)–(23).

Finally, we also mention a natural extension of our new element to three dimensions. The three-dimensional element has eight corner nodes, used for the coordinate, displacement and pressure interpolations,

$$\begin{aligned} \mathbf{x} &= \sum_{i=1}^{8} h_i(\mathbf{r})\mathbf{x}_i\,, \\ \mathbf{u} &= \sum_{i=1}^{8} h_i(\mathbf{r})\mathbf{u}_i\,, \\ p &= \sum_{i=1}^{8} h_i(\mathbf{r})p_i\,. \end{aligned} \tag{27}$$

The interpolation matrix for the enhancement in strains, considering the $2\times2\times2$ element is,

$$\mathbf{G}^*(\mathbf{r}) = \begin{pmatrix} r & 0 & 0 & 0 & 0 & 0 & 0 & 0 & 0 & rs & 0 & 0 & rt & 0 & 0 \\ 0 & s & 0 & 0 & 0 & 0 & 0 & 0 & 0 & 0 & sr & 0 & 0 & st & 0 \\ 0 & 0 & t & 0 & 0 & 0 & 0 & 0 & 0 & 0 & 0 & tr & 0 & 0 & ts \\ 0 & 0 & 0 & r & s & 0 & 0 & 0 & 0 & 0 & 0 & 0 & 0 & 0 & 0 \\ 0 & 0 & 0 & 0 & 0 & r & t & 0 & 0 & 0 & 0 & 0 & 0 & 0 & 0 \\ 0 & 0 & 0 & 0 & 0 & 0 & 0 & s & t & 0 & 0 & 0 & 0 & 0 & 0 \end{pmatrix} \tag{28}$$

and the general interpolation matrix $\mathbf{G}(\mathbf{r})$ is given by Eq. (21) using the appropriate transformation matrix $\bar{\mathbf{X}}_0$.

3. The Numerical Inf-Sup Test

In the numerical inf-sup test we choose an analysis problem and investigate whether the inf-sup values in the finite element solutions of that problem with increasing finer meshes are bounded. We use here the cantilever problem shown in Fig. 1.

We write the inf-sup condition as follows[3]:

$$\inf_{q_h\in P_h(D_h)} \sup_{\mathbf{v}_h\in V_h} \frac{\int_V q_h \operatorname{div}(\mathbf{v}_h)\, dV}{\|q_h\|\,\|\mathbf{v}_h\|_1} \geq \alpha > 0\,, \tag{29}$$

where α is a constant independent of the element size h and the bulk modulus κ. V_h is the space in which we seek our finite element solution,

$$V_h = \left\{ \mathbf{v}_h : \frac{\partial v_{h_i}}{\partial x_j} \in L^2,\ \ i,j = 1,2,3 \right\} \tag{30}$$

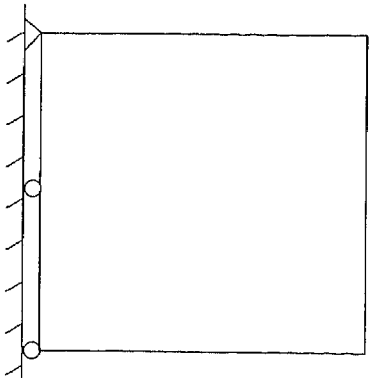

Fig. 1. Inf-sup test. Problem considered.

and D_h is defined as

$$D_h = \{\mathrm{div}(\mathbf{v}_h) : \mathbf{v}_h \in V_h\}\,. \tag{31}$$

$P_h(D_h)$ is the L^2-projector onto the auxiliary space Q_h which we identify as our pressure space, see Eq. (9). The symbol $\|\cdot\|$ stands for the L^2-norm and

$$\|\cdot\|_1 = \int_V \sum_{i,j=1}^{3} \left(\frac{\partial(\cdot)_i}{\partial x_j}\right)^2 dV\,. \tag{32}$$

In order to obtain the inf-sup value (i.e. the left-hand side in Eq. (29)) numerically for a given mesh we write the relation (29) in terms of the unknown nodal values instead of the fields[3]

$$\inf_{\mathbf{W}_h} \sup_{\mathbf{V}_h} \frac{\mathbf{W}_h^T \mathbf{G}_h \mathbf{V}_h}{\sqrt{\mathbf{W}_h^T \mathbf{G}_h \mathbf{W}_h}\sqrt{\mathbf{V}_h^T \mathbf{S}_h \mathbf{V}_h}} \geq \alpha > 0\,, \tag{33}$$

where

$$\mathbf{V}_h^T \mathbf{S}_h \mathbf{V}_h = \int_V \sum_{i,j=1}^{3} \frac{\partial v_{h_i}}{\partial x_j}\frac{\partial v_{h_i}}{\partial x_j}\, dV \tag{34}$$

$$\mathbf{W}_h^T \mathbf{G}_h \mathbf{V}_h = \int_V \mathrm{div}(\mathbf{w}_h) P_h(\mathrm{div}\ \mathbf{v}_h)\, dV \tag{35}$$

and solve the eigenproblem[3]

$$\mathbf{G}_h \mathbf{V}_h = \lambda \mathbf{S}_h \mathbf{V}_h. \tag{36}$$

Let us call λ_p the first nonzero eigenvalue. Then the inf-sup value is simply $\sqrt{\lambda_p}$, and we require that for any sequence of meshes this value is bounded by α. Also, the number of zero eigenvalues determines whether spurious pressure modes are present.

The key is the evaluation of the matrices $\mathbf{G}_h$ and $\mathbf{S}_h$. Consider the matrix problem that corresponds to the variational formulation defined in Eqs. (9),

$$\begin{pmatrix} \mathbf{A}_h & \mathbf{B}_h^T \\ \mathbf{B}_h & -\frac{1}{\kappa}\mathbf{T}_h \end{pmatrix} \begin{pmatrix} \tilde{\mathbf{U}}_h \\ \mathbf{P}_h \end{pmatrix} = \begin{pmatrix} \tilde{\mathbf{F}}_h \\ \mathbf{0} \end{pmatrix} . \tag{37}$$

From Eq. (17) we can identify

$$\mathbf{A}_h = \begin{pmatrix} (\mathbf{K}_{uu})_h & (\mathbf{K}_{u\alpha})_h \\ (\mathbf{K}_{u\alpha})_h^T & (\mathbf{K}_{\alpha\alpha})_h \end{pmatrix} , \tag{38}$$

$$\mathbf{B}^T{}_h = \begin{pmatrix} (\mathbf{K}_{up})_h \\ (\mathbf{K}_{\alpha p})_h \end{pmatrix} , \tag{39}$$

$$\mathbf{T}_h = \int_V \mathbf{H}^T(\mathbf{r})\mathbf{H}(\mathbf{r})dV , \tag{40}$$

$$\tilde{\mathbf{U}}_h = \begin{pmatrix} \hat{\mathbf{u}} \\ \boldsymbol{\alpha} \end{pmatrix} , \tag{41}$$

$$\mathbf{P}_h = \tilde{\mathbf{p}} , \tag{42}$$

$$\tilde{\mathbf{F}}_h = \begin{pmatrix} \mathbf{R}(\mathbf{u}) \\ \mathbf{0} \end{pmatrix} , \tag{43}$$

$\mathbf{G}_h$ is now directly obtained from,[3]

$$\mathbf{G}_h = \mathbf{B}_h^T \, \mathbf{T}_h^{-1} \, \mathbf{B}_h . \tag{44}$$

Note that externally applied loads and material parameters do not affect the expressions in Eqs. (34)–(36).

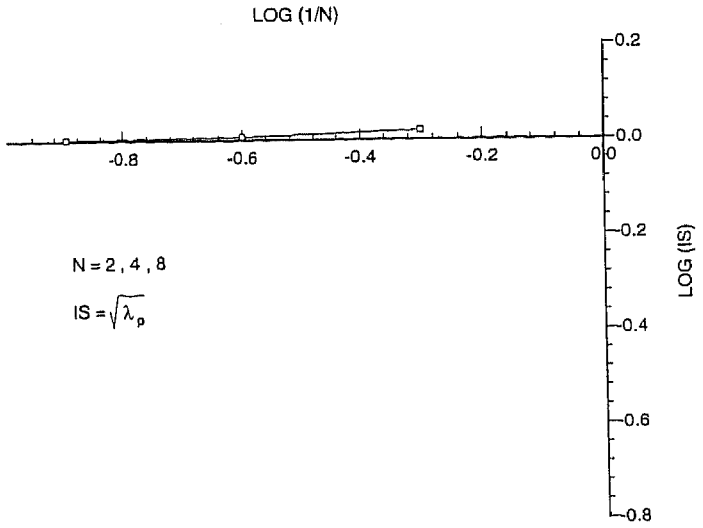

Fig. 2. Results of the inf-sup test, N is the number of elements on each side of the plate in Fig. 1.

The evaluation of $\mathbf{S}_h$ must include the fact that we are interpolating not only the displacements but also strains. Making use of Korn's inequality[4] we therefore use instead of the one-norm defined in Eq. (32) and evaluated in Eq. (34), an equivalent norm defined in terms of the components of the strain tensor,

$$|\mathbf{v}| = \left(\sum_{i,j=1}^{3} \|\varepsilon_{ij}\|^2 \right)^{1/2}. \tag{45}$$

Figure 2 shows the result of the test applied to the problem shown in Fig. 1. The evaluation of the inf-sup value was performed for three uniform meshes in which $N = 2, 4, 8$ where N is equal to the number of elements on each side. $IS = \sqrt{\lambda_p}$, where λ_p is the smallest nonzero eigenvalue. The figure shows that the test is passed. Also, the counts of the number of zero eigenvalues showed that spurious modes are not present.

4. Numerical Tests

We present the results of four numerical tests to demonstrate the capabilities of the element.

4.1. *Beam bending*

A beam clamped at one end and subjected to an applied moment at the other end is modeled using two finite elements. The mesh is distorted by rotating the common

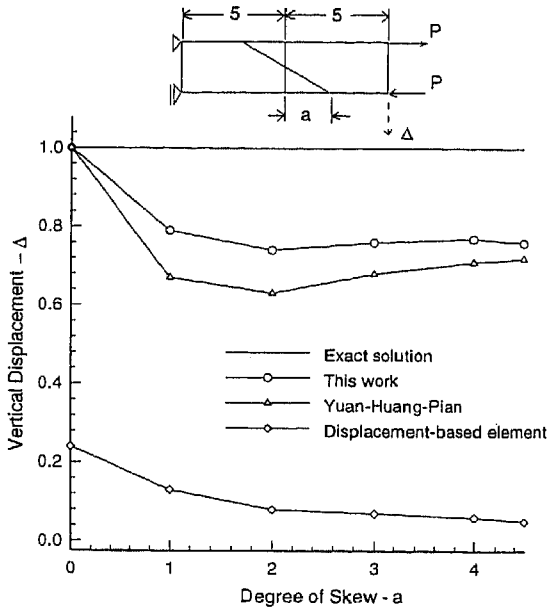

Fig. 3. Bending test, Poisson's ratio = 0.

edge of the elements. This is a classical test to evaluate the capabilities of elements when subjected to distortions. Figure 3 shows the calculated results in comparison with the analytical solution as a function of the degree of skew.

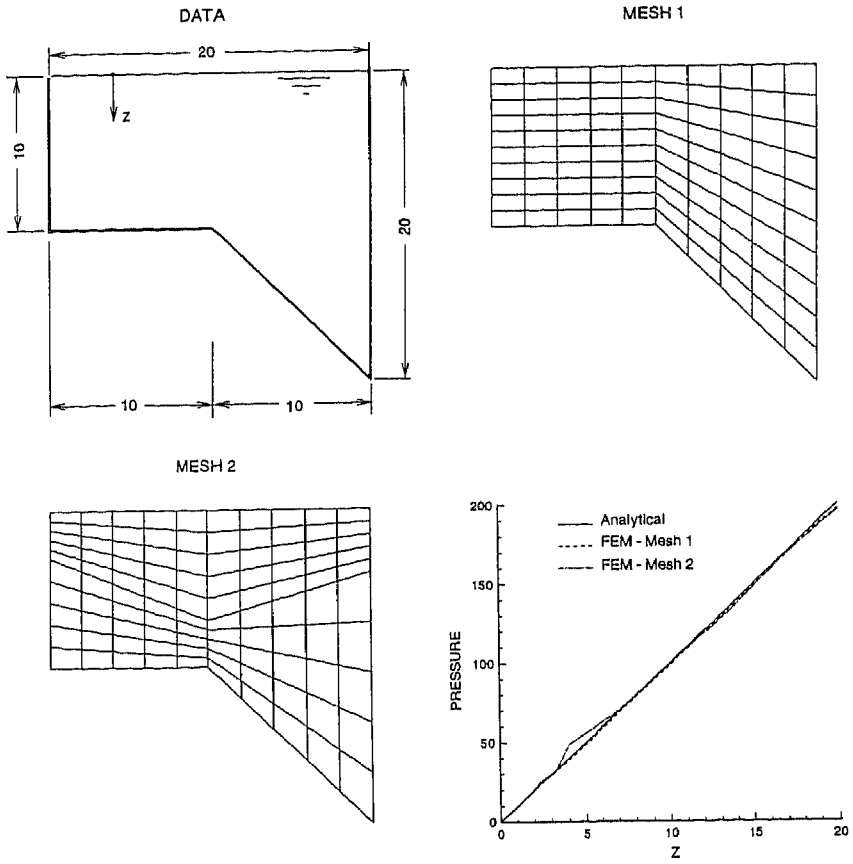

Fig. 4. No-flow test.

4.2. *No-flow test*

An almost incompressible solid/fluid rests in a nonsquare cavity subjected to gravity loading, see Fig. 4. The displacements velocities normal to the walls are prescribed to be zero and the pressure at the free surface is $p = 0$. The solution must give zero displacements /velocities and a linear distribution in pressure. Our numerical results give negligible displacements/velocities (because we are using an almost incompressible material) and an almost linear distribution in pressure as shown in the figure. The deviation from linearity is larger when distorted elements are used.

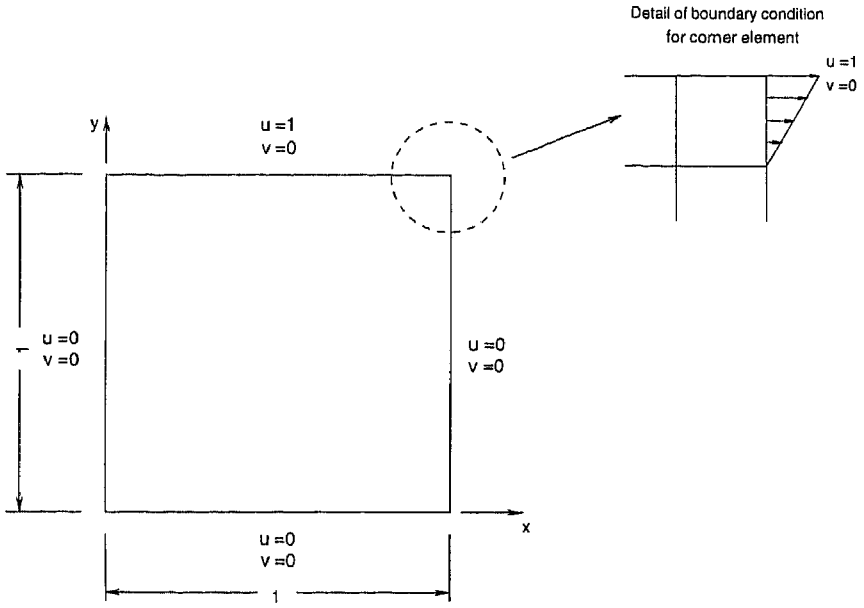

Fig. 5. Driven cavity, boundary condition at corner element.

4.3. *Driven cavity*

A square cavity with boundary velocities constrained to zero along three edges and a uniformly prescribed velocity applied along the top edge is considered, see Fig. 5. The pressure distribution compared with the 9/4-c (or Q2-Q1) element (that is, the biquadratic velocity and bilinear continuous pressure element) as well as pressure band plots are shown in Fig. 6 for 10×10 and 20×20 meshes, respectively.

4.4. *Axisymmetric cylinder under internal pressure*

To test the axisymmetric element we consider a thick cylinder of infinite length so that it cannot expand in the z direction. The internal radius is $R_\mathrm{i} = 1$ and outer radius is $R_\mathrm{o} = 2$. The internal pressure is $p = 6$ and the material parameters are Young's modulus $E = 1000$ and Poisson's ratio $\nu = 0.4999$. The analytical solution for this problem is

$$u = \frac{(1+\nu)\, p\, R_\mathrm{i}^2}{E\,(R_\mathrm{o}^2 - R_\mathrm{i}^2)} \left[\frac{R_\mathrm{o}^2}{r} + (1-2\nu)\, r \right], \tag{46}$$

$$p = \frac{2}{3} \frac{p\, R_\mathrm{i}^2\, (1+\nu)}{R_\mathrm{i}^2 - R_\mathrm{o}^2}. \tag{47}$$

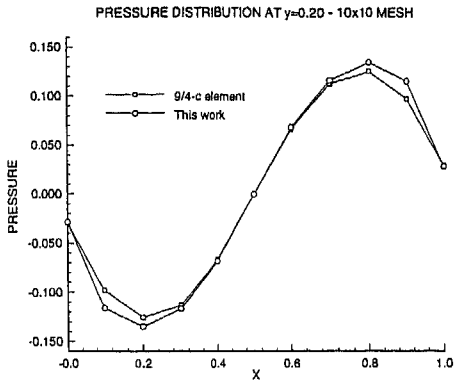

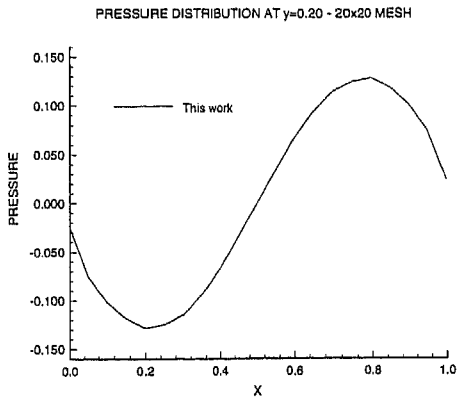

(a) Driven cavity. Incompressible flow.

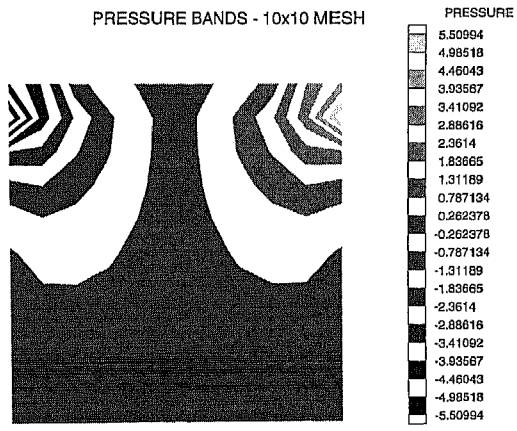

(b)

Fig. 6.

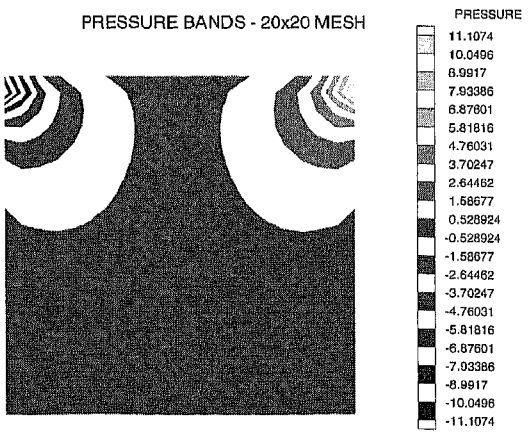

(c)

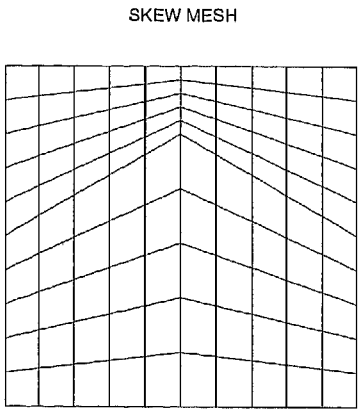

(d)

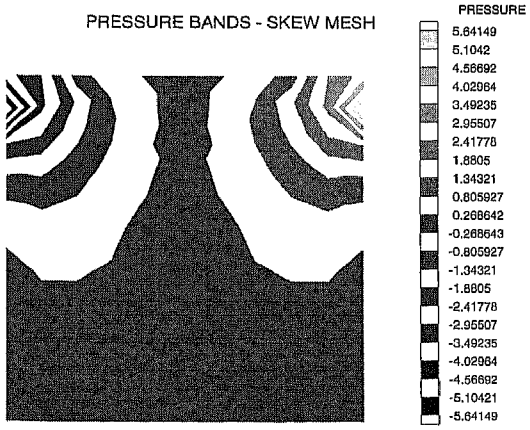

(e)

Fig. 6. (*Continued*)

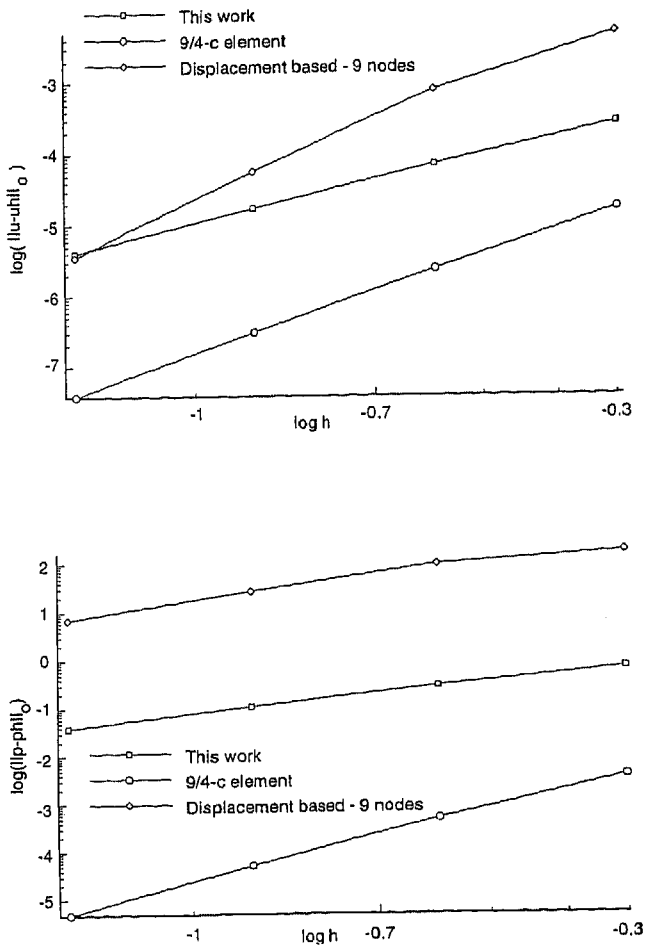

Fig. 7. Cylinder under internal pressure. Convergence rates.

We studied the rates of convergence for this rather simple case and show in Fig. 7 the L_2 norms of the analytical displacement minus the finite element displacement and the analytical pressure minus the finite element pressure as a function of the mesh size h.

We note that in this analysis, the proposed element converges with order 2 in the displacement norm and an order larger than 1 in the pressure norm. It is also interesting to compare the performance with the convergence of the 9/4-c element (the Q2-Q1 element) and the displacement-based element. The order of displacement convergence of both nine-node elements is 3, but the error using the displacement-based element is much larger. Considering that $\|\mathbf{u} - \mathbf{u}_h\|_0 = c\ h^3$, this error is due to a large constant c, typical of the locking behavior.

5. Concluding Remarks

We have presented a four-node quadrilateral element with good predictive capabilities in structural bending problems and in the analysis of almost incompressible media (solids and fluids). The results presented for various example problems show the behavior of the element.

A numerical inf-sup test of the element in incompressible analysis was also performed and the element passes this test. While the numerical results given in the paper indicate that the element has good predictive capability, a full mathematical analysis of the convergence behavior of the element would be valuable.

References

1. K. J. Bathe, **Finite Element Procedures** (Prentice Hall, 1995).
2. F. Brezzi and M. Fortin, **Mixed and Hybrid Finite Element Methods** (Springer-Verlag, 1991).
3. D. Chapelle and K. J. Bathe, *The inf-sup test, Comput. Structures* **47** (1993) 537-545.
4. P. G. Ciarlet, **The Finite Element Method for Elliptic Problems** (North-Holland, 1978)
5. E. N. Dvorkin and S. I. Vasolo, *A quadrilateral 2d finite element based on mixed interpolation of tensorial components, Engrg. Comput.* **6** (1989) 217–224.
6. J. C. Simo and M. S. Rifai, *A class of mixed assumed strain methods and the method of incompatible modes, Internat. J. Numer. Methods Engrg.* **29** (1990) 1595–1638.
7. E. L. Wilson and A. Ibrahimbegovic, *Use of incompatible displacement modes for the calculation of element stiffness and stresses, Finite Element Anal. Design* **7** (1990) 229–241.
8. K. Yuan, Y. Huang and T. H. H. Pian, *New strategy for assumed stress for 4-node hybrid stress membrane element, Internat. J. Numer. Methods Engrg.* **36** (1993) 1747–1763.